LETTER

Self-Assembled Chitosan Nanotemplates for Biomineralization of Controlled Calcite Nanoarchitectures

Jingming Gong,*,†,‡ Zhengji Zhou,†,§ Xianluo Hu,† Man-keung Wong,‡ Ka-wai Wong,*,† and Zuliang Du§

Key Laboratory of Pesticide & Chemical Biology of Ministry of Education, College of Chemistry, Central China Normal University, Wuhan 430079, China, Department of Physics, The Chinese University of Hong Kong, Shatin, New Territories, Hong Kong, China, and Laboratory for Special Functional Materials, Henan University, Kaifeng, Henan 475001, China

ABSTRACT Three-dimensional chitosan self-assembled nanostructures are reported whose morphology can be adjusted by tuning of the processing parameters, including the rate of solvent removal, the surface roughness of the substrate, and the polarity of the solvent used. Upon this, chitosan nanostructures of more interesting morphology and even higher complexity can be prepared, which can serve as nanotemplates for subsequent biomineralization of calcium carbonate, leading to controllable three-dimensional biominerals having the same complex morphology as that exhibited by the self-assembled chitosan nanotemplates.

KEYWORDS: chitosan • self-assembly • biomineralization • calcium carbonate

Inspired by the fascinating, and at the same time functional, three-dimensional (3D) calcium carbonate ($CaCO_3$) biominerals observed in nature (e.g., echinoderms (1) and coccoliths (2)), bottom-up biomineralization for the preparation of crystalline calcite micro- and nanostructures has aroused enormous interest and effort from scientists worldwide. Not just limited to their eye-catching appearance, these 3D calcite skeletons bear significant technological impact in various biological applications and nanodevices (e.g., electronic, optical, optoelectronic, sensory) (1, 3, 4). Previously, generations of 3D calcite crystals were reported by using photolithographically patterned silicon with metallic micro- or even nanopatterns (4). This technique involves complicated lithographic processes. Also, the final calcite structures are restricted to those accessible forms from lithographic techniques. A layer-by-layer approach using a polymeric mediator was another commonly adapted technique to prepare more complicated biomineral structures (5). Usually, nacre or mesoscale structures were deduced without specific nanomorphology. Recently, Qi reported an elegant method for preparing 3D-ordered macroporous calcite crystals using ordered colloidal crystals of polymeric microspheres as templates (6). However, all product structures were limited to the basis of inverse opal. Biomorphic templating represents another viable method for generating 3D calcite (7). Despite the ease of preparation, the final morphology is controlled by the choice of biotemplate used rather than the experimental processing conditions. Fabrication of 3D calcite crystals of higher morphological complexity in a controllable fashion by a simple enough preparation process remains a serious challenge to material chemists.

In this letter, we reported the construction of 3D self-assembled (SA) chitosan nanostructures. The morphology of the SA chitosan nanostructures was found to be controllable by tuning of the experimental processing parameters, e.g., the rate of solvent removal, surface conditions of the substrate, and choice of the solvent. They then served as nanotemplates for biomineralization of calcite nanoarchitectures. Chitosan, a deacetylation product of chitin and a naturally occurring biopolymer, is a functional and basic polysaccharide composed of β-1,4-linked glucosamine (8). Owing to its special properties like nontoxicity, biodegradability, biocompatibility, and antimicrobial activity (8, 9), this polycationic biopolymer is receiving a great deal of attention for biosensing, biomineralization, and medical and pharmaceutical applications (9, 10). Chitosan micro- or nanofibers have been widely accepted as biomedical scaffolding materials to restore, maintain, or improve the functions of various tissues (11). Therefore, the preparation of 3D chitosan nanostructures with controllable morphology is highly desirable but so far has met with limited success. Recently, we reported an electrochemical approach to synthesizing different chitosan one-dimensional nanostructures (nanowires, nanotubes, and nanorods) with the aid of an external electric field (12). In the present article, the preparation of 3D calcite crystals of higher morphological complexity in a controllable fashion by a simple SA approach will be described. To the best of our knowledge, this is the first report

* Corresponding author. E-mail: kwwong@cuhk.edu.hk (K.-w.W.), jmgong@mail.ccnu.edu.cn (J.G.).
Received for review August 18, 2008 and accepted October 27, 2008
† Central China Normal University.
‡ The Chinese University of Hong Kong.
§ Henan University.
DOI: 10.1021/am8000055

Published on Web 11/24/2008

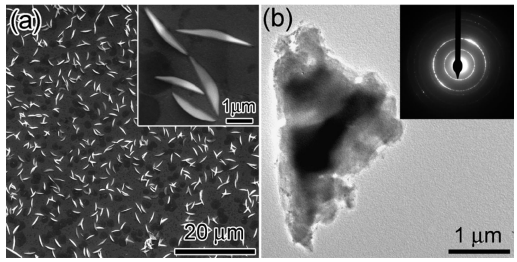

FIGURE 1. (a) SEM image of SA chitosan in ethanol, dried at 65 °C in air. Inset of part a: enlarged SEM image showing a bladelike structure of SA chitosan. (b) TEM image of a typical chitosan NB. Inset of part b: SAED pattern of the chitosan NB in part b.

on finely controlling chitosan nanostructures by a SA approach. The synthetic process is simple and can be performed under the usual experimental laboratory conditions.

Chitosan with a ≥75% degree of deacetylation and an average molecular weight of 660 000 as determined by the intrinsic viscosity was obtained from Sigma. Propylene carbonate (PC; 99.7%, Sigma) was used as received. In a typical experiment, 8.5 mg of chitosan was dispersed into 45 mL of ethanol or PC solution under mild ultrasonication (70 W) for 2 h. The solutions were kept at a pH of ∼4.0 by adding dropwise an appropriate amount of aqueous H_2SO_4. SA chitosan nanostructures were then formed by drop-casting 100 μL of a chitosan solution onto various indium−tin oxide (ITO) substrates. ITO substrates were chosen because the effect of surface conditions on the morphology of SA chitosan is also of interest in the current work. Because it is expected that an oxide surface can interact strongly with the −OH and $-NH_2$ of chitosan, ITO is an ideal candidate because the surface roughness of ITO can be significantly changed by exposure to different surface treatments, such as oxygen glow discharge, UV/ozone, etc. (13). ITO substrates (1.0 × 1.0 cm^2) used have a sheet resistance of about ∼20 Ω. ITO substrates were routinely cleaned by sonication in a detergent and then rinsing in deionized water and acetone sequentially (S1). Some ITO substrates were further treated by oxygen glow discharge (S2) or UV/ozone (S3). Generally, 100 μL of chitosan in acidified ethanol or PC was drop-casted onto S1, S2, or S3 and was heated at 65 °C in air or in a vacuum oven overnight for complete drying. The general morphology of the products was characterized by scanning electron microscopy (SEM; FEI Quanta 400). Selected-area electron diffraction (SAED) patterns were obtained by using transmission electron microscopy (TEM; Philips CM 120, 120 kV). High-resolution TEM (HRTEM) measurements were performed with a high-resolution transmission electron microscope (Tecnai F20, FEI). The roughness of the substrate surface was measured by using an atomic force microscope (AFM, Nanoscope III). X-ray diffraction (XRD) patterns were collected with a Bruker D8 Advanced diffractometer with high-intensity Cu $K\alpha_1$ irradiation (λ = 1.5406 Å).

Figure 1 shows the representative SEM images of SA chitosan (dried at 65 °C in air) on routinely cleaned ITO (S1). Free-standing nanoblades (NBs) were observed to be uniformly distributed over the substrate. The NBs are uniform in size and dimension, which are all standing up on the substrate. A high-magnification SEM image (inset of Figure 1a) shows that these NBs have an average side length of

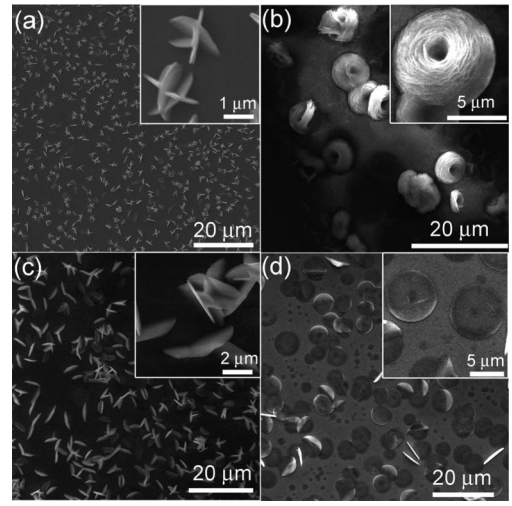

FIGURE 2. SEM images of SA chitosan in an ethanol solvent, film dried at (a) 65 °C, (b) 90 °C in vacuum onto S1, (c) 65 °C in air onto S2, and (d) 65 °C in air onto S3. Inset: corresponding enlarged SEM images.

∼2.0 um, a thickness of ∼100 nm, and a width of ∼500 nm. Figure 1b displays the TEM image of a representative chitosan NB. As shown, the chitosan NB consists of aggregation of multiple smaller pieces. The corresponding SAED pattern is shown in the inset of Figure 1b, which indicates a polycrystalline nature. The bladelike or sheetlike structure observed is consistent with the fact that chitosan prefers to form layered molecular structures owing to the presence of hydroxyl and amino groups, which induce both strong inter- and intramolecular hydrogen-bonding interactions between chitosan molecules (14). Similar behavior was also reported for the SA systems of *N*-alkylacrylamide polymer and bisurea-based organogels (15). However, when we dried the drop-cast chitosan solution by vacuum heating instead of standalone air drying, those monodispersed individual NBs tended to assemble quickly and interlacement was observed. Interlaced NBs were homogeneously standing on the substrates (Figure 2a). Upon a further increase of the vacuum drying temperature to 90 °C, flower-like nanostructures, composed of multilayered NBs, were observed (Figure 2b). A higher rate of solvent removal was induced by an increased vacuum drying temperature, which directly prompts the self-assembling rate of chitosan, resulting in the interlaced 3D architecture. Further interlacements of NBs at a faster rate of solvent removal eventually result in a flower-like morphology, with assembly of multiply stacked NBs. Evidently, the rate of solvent removal strongly affects the SA behavior of chitosan, which, in turn, leads to different 3D chitosan nanoarchitectures. Further investigations were made to examine the control over the nanomorphology by changing two other experimental conditions: the surface conditions of the substrate and the choice of the solvent.

ITO substrates further treated by oxygen glow discharge plasma (S2) or UV/ozone (S3) were used. Parallel studies showed that both treatments could effectively remove surface hydrocarbon contaminants and introduce fully oxidized ITO surfaces. Both exhibit almost the same contact angle toward ethanol, implying a nearly identical macroscopic solution/surface interaction. Despite their similarity in a

macroscopic point of view, AFM measurement revealed a significant difference in the surface roughness. Because energetic oxygen species were involved in oxygen glow discharge plasma, the corresponding ITO surface suffered severe ion bombardment during treatment, while a surface smoothing effect was observed by the UV/ozone treatment as reported by Li et al. (13) ITO substrates treated by oxygen glow discharge plasma possessed a roughened surface with a root-mean-square roughness of 1.169 nm, compared to 0.218 and 1.061 nm for ITO surfaces treated by UV/ozone and routine cleaning procedures. The corresponding SEM images of SA chitosan nanostructures (dried at 65 °C in air) on S2 and S3 are shown in Figure 2c,d. Chitosan NBs were again observed standing upright on the ITO substrate of S2, as on S1 (after routine cleaning). However, on S3 (substrate treated by UV/ozone), NBs and disks were found lying on the substrate instead of standing. Because the hydroxyl and amino groups along the chitosan molecular chains can interact strongly with the oxygen-containing functional groups (e.g., −O− and −OH) on ITO, a smoother surface in the microscopic level can promote surface nucleation and growth of chitosan species, leading to flat structures lying on the substrate (Figure 2d). However, for rougher surface (as for S1 and S2), standing structures are more favorable because intimate contacts between chitosan and ITO are mostly restricted to those with the protruding areas and points of the ITO surface. As such, upright SA chitosan nanostructures were observed on the much rougher S1 and S2.

Besides the rate of solvent removal and the roughness of the substrate surface, the solvent effect was also investigated. When PC was used instead of ethanol for the preparation of SA chitosan here, nanorods (NRs) with an average diameter and length of 120 nm and 1.25 μm, respectively (Figure 3a,b) were found on the routinely cleaned ITO, instead of NBs. It was proposed in our previous study (12) that nanoscale embryos play a vital role in the generation of subsequent nanostructures. We, therefore, carefully examined the embryos collected in solutions of chitosan in ethanol and in PC. As-received chitosan powder was first introduced into acidified PC or ethanol solution (pH adjusted to ~4.0) under mild ultrasonication. Chitosan embryos were collected by copper grids for subsequent TEM. Parts c and d and parts e and f of Figure 3 show the TEM images of chitosan embryos formed and collected in ethanol and in PC, respectively. For chitosan in ethanol, embryos with shells or stacked layers are clearly observed. It is consistent with the report by Okuyama et al. that molecular layer stacking is more likely adapted by chitosan, leading to a layered structure bounded by the intra- and intermolecular hydrogen bonds (14). It is proposed that further growth of these shelled and layered embryos resulted in small pieces that aggregated into larger sheetlike and bladelike structures with in-plane randomness. The corresponding SAED thus displays a polycrystalline nature rather than a single-crystalline nature, which requires extension of order of molecular arrangement over the entire system. Formation of a single-crystalline or highly oriented structure is rather difficult for

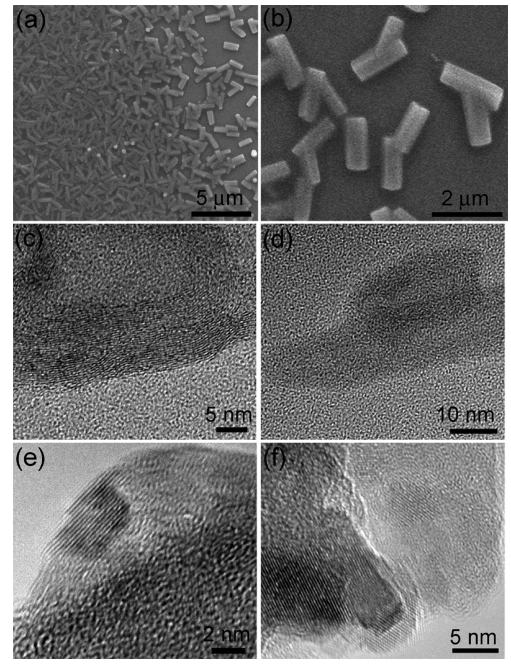

FIGURE 3. (a and b) SEM images of SA chitosan in PC solvent, film dried at 65 °C in air. HRTEM images of the embryos collected from the solutions of chitosan in (c and d) ethanol and nd f) PC as the solvent, respectively.

the round and curved shell-like layered embryonic structures in the case for sheetlike and bladelike SA chitosan structures. As such, upon further growth, sheetlike structures will be evolved in the SA process. When the solvent was replaced by PC (with other experimental conditions being kept unchanged), crystalline particle-like embryos were observed with an average diameter of 2 nm (Figure 3e,f). These regular, crystalline particle-like embryos are expected to follow oriented attachment as proposed by Penn et al. (16), i.e., the spontaneous self-organization of adjacent particles, followed by joining of particles at a common planar interface, which is nowadays a well-established mechanism to explain the growth of anisotropic, wire/chainlike nanostructures (17). The difference in embryo morphology between the use of ethanol and PC as solvents is attributed to the fact that PC is more polar than ethanol. The dipole of PC is 4.98 D, while that of ethanol is only 1.69 D (18). The more polar PC can act better as a surfactant to minimize the surface free energy of chitosan embryos, which favors the formation of crystalline particle-like chitosan embryos. However, when ethanol is used to solvate the chitosan, owing to its much lower polarity for strong interaction with the chitosan molecules, the chitosan molecules prefer to aggregate, forming a layered structure by molecular stacking as usual. This demonstrates the effect of solvent on the morphology of initial chitosan embryos, which in turn crucially affects the shape and configuration of the final SA chitosan nanostructures.

Undoubtedly, 3D chitosan nanostructures can be prepared by a simple SA process. The exact shape and morphology can be adjusted by varying (i) the rate of solvent removal, (ii) the surface roughness of the substrate, and (iii) the polarity of the solvent used, as shown by the study described above. These 3D SA chitosan nanostructures were

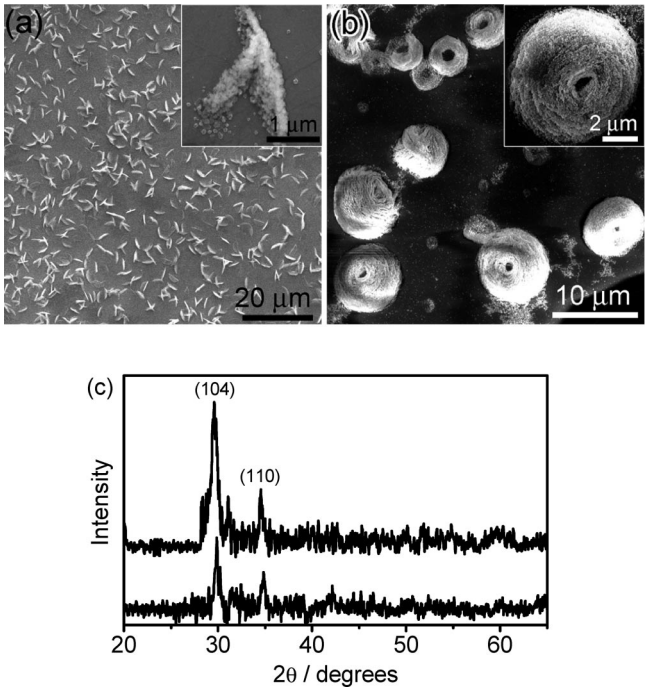

FIGURE 4. (a and b) SEM images of $CaCO_3$ prepared from SA chitosan nanostructures as shown in parts a and b of Figure 2, respectively. (c) XRD pattern of the as-prepared $CaCO_3$.

then subjected to biomineralization of $CaCO_3$. Biomineralization was performed on these SA chitosan nanotemplates from a supersaturated aqueous solution of calcium carbonate. First, a supersaturated $CaCO_3$ solution was prepared by continuously pumping CO_2 into a flask of deionized water containing as-purchased pure $CaCO_3$ powder until all $CaCO_3$ dissolved and resulted in a supersaturated $CaCO_3$ solution at a concentration of 0.5 mmol/L. Second, ITO substrates coated with SA chitosan were immersed into the supersaturated aqueous solution of $CaCO_3$ for 24 h. Biomineralization occurred upon solvent and CO_2 evaporation. Finally, the samples were taken out for drying in air at room temperature. Parts a and b of Figure 4 show the biomineralized nanoarchitectures prepared from SA chitosan nanostructures fabricated as those shown in parts a and b of Figure 2. Evidently, the biomineralized products perfectly dictate the SA chitosan nanotemplates, leading to $CaCO_3$ biominerals in the form of interlaced NBs, as well as flower-like structures. XRD studies reveal that both are calcite (Figure 4c), with the characteristic reflection at $2\theta = 29.6°$, corresponding to the hexagonal crystal structure of $CaCO_3$ (JCPDS no. 81-2027). This implies that $CaCO_3$ preferentially nucleated and grew around the SA chitosan nanotemplates, giving exactly the same morphology. This phenomenon is attributed to the preferred adsorption of ions like Ca^{2+} and CO_3^{2-} on the SA chitosan backbone, which possesses surface charges and strong polarity for attraction of ions and polar species. When more 3D SA chitosan nanotemplates of even higher complexity and variety are prepared by adjusting individual processing parameters and/or a combination of them, highly complex 3D calcite biominerals can be obtained in a controllable manner.

3D SA chitosan nanostructures are reported whose morphology can be easily adjusted by tuning of the processing parameters in the SA process. Upon this, chitosan nanostructures of more interesting morphology and even higher complexity can be prepared, which can serve as nanotemplates for subsequent $CaCO_3$ biomineralization, leading to controllable 3D biominerals having the same complex morphology as that exhibited by the SA chitosan nanotemplates. In addition, they provide a variety of nanomorphologies for further applications and development in biological and biomedical studies, for example, cell adhesion, a natural extracellular matrix to mimic biomineralization, nanostructure-based biosensors, tissue-compatible scaffolds, etc.

Acknowledgment. J.G. is thankful for support by the National Natural Science Foundation of China (Grant 20803026), and K.-w.W. acknowledges support by the General Research Fund (Project 403708).

REFERENCES AND NOTES

(1) (a) Aizenberg, J.; Tkachenko, A.; Weiner, S. *Nature* **2001**, *412*, 819–822. (b) Aizenberg, J.; Hendler, G. *J. Mater. Chem.* **2004**, *14*, 2066–2072.
(2) Young, J. R.; Davis, S. A.; Bown, P. R.; Mann, S. *J. Struct. Biol.* **1999**, *126*, 195–215.
(3) (a) Dujardin, E.; Mann, S. *Adv. Mater.* **2002**, *14*, 775–788. (b) Park, R. J.; Meldrumb, F. C. *Adv. Mater.* **2002**, *14*, 1167–1169. (c) Wucher, B.; Yue, W.; Kulak, A. N.; Meldrum, F. C. *Chem. Mater.* **2007**, *19*, 1111–1119.
(4) (a) Aizenberg, J.; Muller, D. A.; Grazul, J. L.; Hamann, D. R. *Science* **2003**, *299*, 1205–1208. (b) Aizenberg, J. *Adv. Mater.* **2004**, *16*, 1295–1302.
(5) (a) Wei, H.; Ma, N.; Shi, F.; Wang, Z.; Zhang, X. *Chem. Mater.* **2007**, *19*, 1974–1978. (b) Xu, A. W.; Antonietti, M.; Yu, S. H.; Cölfen, H. *Adv. Mater.* **2008**, *20*, 1333–1338. (c) Kato, T. *Adv. Mater.* **2000**, *12*, 1543–1546.
(6) Li, C.; Qi, L. M. *Angew. Chem., Int. Ed.* **2008**, *47*, 2388–2393.
(7) Zheng, Z.; Huang, B. J.; Ma, H. Q.; Zhang, X. P.; Liu, M. Y.; Liu, Z.; Wong, K. W.; Lau, W. M. *Cryst. Growth Des.* **2007**, *7*, 1912–1917.
(8) (a) Park, S. B.; You, J. O.; Park, H. Y.; Haam, S. J.; Kim, W. S. *Biomaterials* **2001**, *22*, 323–330. (b) Mehrdad, Y. P.; Jaime, R.; Raul, Q. *Macromol. Chem. Phys.* **2000**, *201*, 923–930.
(9) (a) Luo, X. L.; Xu, J. J.; Wang, J. L.; Chen, H. Y. *Chem. Commun.* **2005**, *16*, 2169–2171. (b) Langer, R. A. *Chem. Res.* **2000**, *33*, 94–101.
(10) (a) Langer, R.; Tirrell, D. A. *Nature* **2004**, *428*, 487–492. (b) Kumar, M. N.; Muzzarelli, R. A.; Muzzarelli, C.; Sashiwa, H.; Domb, A. J. *Chem. Rev.* **2004**, *104*, 6017–6084.
(11) (a) Kumar, M. N. *React. Funct. Polym.* **2000**, *46*, 1–27. (b) Park, Y. J.; Lee, Y. M.; Park, S. N.; Sheen, S. Y.; Chung, C. P.; Lee, S. J. *Biomaterials* **2000**, *21*, 153–159. (c) Tamura, H.; Tsuruta, Y.; Itoyama, K.; Worakitkanchanakul, W.; Rujiravanit, R.; Tokura, S. *Carbohydr. Polym.* **2004**, *56*, 205–211.
(12) Gong, J. M.; Hu, X. L.; Wong, K. W.; Zheng, Z.; Yang, L.; Lau, W. M.; Du, R. *Adv. Mater.* **2008**, *20*, 2111–2114.
(13) Li, C. N.; Djurišić, A. B.; Kwong, C. Y.; Lai, P. T.; Chan, W. K.; Liu, S. Y. *Appl. Phys. A: Mater. Sci. Process.* **2005**, *80*, 301–307.
(14) Okuyama, K.; Noguchi, K.; Miyazawa, T.; Yui, T.; Ogawa, K. *Macromolecules* **1997**, *30*, 5849–5855.
(15) (a) Davis, R. J.; Berger, R.; Zentel, R. *Adv. Mater.* **2007**, *19*, 3878–3881. (b) Endo, H.; Mitsuishi, M.; Miyashita, T. *J. Mater. Chem.* **2008**, *18*, 1302–1308.
(16) (a) Penn, R. L.; Banfield, J. F. *Science* **1998**, *281*, 969–971. (b) Banfield, J. F.; Welch, S. A.; Zhang, H.; Ebert, T. T.; Penn, R. L. *Science* **2000**, *289*, 751–754.
(17) (a) Tang, Z. Y.; Kotov, N. A.; Giersig, M. *Science* **2002**, *297*, 237–240. (b) Pacholski, C.; Kornowski, A.; Weller, H. *Angew. Chem., Int. Ed.* **2002**, *41*, 1188–1191. (c) Giersig, M.; Pastoriza-Santos, I.; Liz-Marzan, L. M. *J. Mater. Chem.* **2004**, *14*, 607–610. (d) Lu, W. G.; Gao, P. X.; Bin, J. W.; Wang, Z. L.; Fang, J. Y. *J. Am. Chem. Soc.* **2004**, *126*, 14816–14821.
(18) Lide, D. R. *Handbook of Organic Solvents*; CRC Press: Boca Raton, FL, 1995; pp 205. and 412.

AM8000055